

Hypothetical neural control of human bipedal walking with voluntary modulation

Sungho Jo

Received: 21 March 2007 / Accepted: 4 October 2007
© International Federation for Medical and Biological Engineering 2007

Abstract A hypothetical neuromusculoskeletal model is developed to simulate human normal walking and its modulated behaviors. A small set of neural periodic patterns drive spinal muscle synergies which in turn lead to specific pattern of muscle activation and supraspinal feedback systems maintain postural balance during walking. Then, the model demonstrates modulated behaviors by superimposing voluntary perturbations on the underlying walking pattern. Motions of kicking a ball and obstacle avoidance during walking are simulated as examples. The superposition of the new pulse command to a set of invariant pulses representing spino-locomotor is sufficient to achieve the coordinated behaviors. Also, forward bent walking motion is demonstrated by applying similar superposition. The composition of activations avoids a complicated computation of motor program for a specific task and presents a simple control scheme for different walking patterns.

Keywords Human bipedal walking · Voluntary modulation · Synergy · Cerebro-cerebellar feedback system · Hierarchical neural control

1 Introduction

Burgeoning interest in bipedal robot design as well as in the physiology of human locomotion has stimulated computational investigations of locomotor control. A range of studies have identified underlying patterns of kinematics and muscular activation [25, 34, 39, 40]. Computational locomotion models such as biped, quadruped, or snake-like sliding have principally included neural pattern generators [7, 15, 34, 39]. By using pattern generators those models have successfully implemented realistic locomotion. For example, Taga proposed biped walking models to implement nominal walking behaviors [39] and modulated behaviors during obstacle avoidance as well [40]. Taga's model realizes periodic gaits by interaction between neural rhythmic generator and rhythmic movement of body system, and furthermore, modification of gait pattern by the effect of the discrete movement generator. The neural controller depends on a sequence of global states in terms of body's center of mass and center of pressure. However, most models such as Taga's do not intend to investigate the explicit architecture of the central nervous system (CNS) though proposing biologically inspired paradigms. The nature of neural control of locomotion still remains essentially unexplored. On the other hand, neurophysiological studies indicate that the integrated control of cerebral cortex and cerebellum is influential in, at least, bipedal walking [10, 35, 38]. Bipedal walking is especially challenging because stability maintenance becomes critical. It was shown that realistic control of upright balance can be achieved by stabilized long-loop proprioceptive and force feedback [24]. The model is augmented by including spino-locomotor pattern generation [25] to account for the kinematic, dynamic and physiological features of peripheral and central human locomotor control. It appears that

S. Jo (✉)
Media Laboratory, Massachusetts Institute of Technology,
20 Ames Street E15-054, Cambridge, MA 02139, USA
e-mail: shjo@media.mit.edu

S. Jo
Computer Science Department,
Korea Advanced Institute of Science and Technology,
Yuseong-gu, Daejeon 305-701, Republic of Korea

muscle synergies, together with composite signal feedback, enable multi-joint feedback control.

This paper pursues extension of previous investigation to behavioral modulations during walking. One interesting question is about voluntary modulation by supraspinal system during normal walking: what would be a simple and plausible CNS mechanism to generate modulated walking behaviors? This paper proposes a simple neural mechanism that enables such voluntary tasks while its mechanism principle is consistent with previous investigation of balance recovery and normal walking generation [24, 25]. Given that nominal walking motion is implemented by a motor program in CNS, it is hypothesized that the motor program of behavior does not need to be fully recomputed when voluntary perturbation is temporally applied during a gait.

2 Analysis

2.1 Spinomusculoskeletal model

Two legs and one trunk segments jointed at ankle, knee, and hip represent a human body in the sagittal plane. Each leg includes thigh, shank, and foot segments. Each leg incorporates totally nine muscles, three bi-articular and six mono-articular muscles identified in Table 1. The detail of the anthropometry is summarized in Appendix A.

Physically, the knee angle is locked to prevent hyper-extension, and the fact is modeled by

$$\tau_{i,lock} = \begin{cases} \max(K_k(\theta_{i,min} - \theta_i) - B_k\dot{\theta}_i, 0) & \text{if } \theta_i < \theta_{i,min} \\ \min(K_k(\theta_{i,max} - \theta_i) - B_k\dot{\theta}_i, 0) & \text{if } \theta_i > \theta_{i,max} \end{cases} \quad (1)$$

where K_k , and B_k represent respectively spring and damper coefficients, $\theta_{i,min}$ is a minimum knee angle, and $\theta_{i,max}$ is a maximum knee angle, and θ_i is an actual knee angle ($i = 3,4$). For this research, $\theta_{i,min}$ is set to -160 degrees, and $\theta_{i,max}$ to zero degree.

The neural commands from the CNS are converted to muscle activations represented as $\mathbf{act} = [\text{act}_1 \text{ act}_2 \dots \text{act}_9]^T$ through the neuromuscular excitation–activation coupling [13]. The activation of muscle force by neural input occurs according to the low-pass dynamics approximated by:

$$EC(s) = \frac{\rho^2}{(s + \rho)^2} \quad \rho = 30 \text{ rad/s} \quad [13] \quad (2)$$

and

$$\mathbf{act} = EC(s)(\mathbf{u}_\alpha) \quad (3)$$

where \mathbf{u}_α is the alpha motor neuronal command.

When the muscular and ground reaction torques applied to joints are respectively $\tau_M(\Theta, \dot{\Theta}, \mathbf{act})$ and $\tau_R(F_{gx}, F_{gy}, \Theta)$, the body dynamics is represented as:

$$\mathbf{H}(\Theta)\ddot{\Theta} + \mathbf{C}(\Theta, \dot{\Theta}) = \tau_M(\Theta, \dot{\Theta}, \mathbf{act}) + \tau_R(F_{gx}, F_{gy}, \Theta) + \mathbf{G}(\Theta) \quad (4)$$

where $\Theta = [\theta_1 \ \theta_2 \ \theta_3 \ \theta_4 \ \theta_5 \ \theta_6]^T$, $\dot{\Theta} = [\dot{\theta}_1 \ \dot{\theta}_2 \ \dot{\theta}_3 \ \dot{\theta}_4 \ \dot{\theta}_5 \ \dot{\theta}_6]^T$, and $\mathbf{H}(\Theta)$ is the body inertia matrix, $\mathbf{C}(\Theta, \dot{\Theta})$ is the matrix related to centrifugal and Coriolis forces, $\mathbf{G}(\Theta)$ is the gravitational effect matrix, and $\tau_R(F_{gx}, F_{gy}, \Theta)$ is the torque generated by horizontal and vertical reaction forces to the ground at heel and toe.

The detail of modeling the reaction forces is summarized in Appendix B. The dynamic equations were implemented and simulated using Simmechanics in Matlab[®] (Mathworks Inc., Natick, MA, USA).

Muscular torque is the product of the total muscular forces $\mathbf{F}(\mathbf{l}, \mathbf{i}, \mathbf{act})$ and the moment arms according to:

$$\tau_M(\Theta, \dot{\Theta}, \mathbf{act}) = \mathbf{A}^T \mathbf{F}(\mathbf{l}, \mathbf{i}, \mathbf{act}) \quad (5)$$

$$\mathbf{A}^T = \begin{bmatrix} 0 & 0 & 0 & 0 & -a_5 & a_6 & 0 & 0 & a_9^a \\ 0 & 0 & a_3 & -a_4 & 0 & 0 & a_7^k & -a_8^k & -a_9^k \\ -a_1 & a_2 & 0 & 0 & 0 & 0 & -a_7^h & a_8^h & 0 \end{bmatrix} \quad (6)$$

where a_i^* is the estimated average moment arm over the usual range of motion of the i th muscle in Table 1 ($* = a, k$,

Table 1 Length, moment arm, and PCA parameter values of muscles determined from [33] and [41]

| Muscle | Location | Length (m) | Moment arm (m) | PCA (cm ²) |
|-------------------------------|---------------------------------------|------------|----------------------|------------------------|
| (1) IP: Iliopsoas | Mono, hip flexor | 0.35 | 0.132 | 17 |
| (2) GM: Gluteus Maximus | Mono, hip extensor | 0.30 | 0.092 | 30.4 |
| (3) BFS: Biceps femoris short | Mono, knee flexor | 0.29 | 0.049 | 6.8 |
| (4) VA: Vastus | Mono, knee extensor | 0.26 | 0.04 | 30 |
| (5) TA: Tibialis anterior | Mono, ankle dorsi-flexor | 0.30 | 0.023 | 9.1 |
| (6) SO: Soleus | Mono, ankle plantar-flexor | 0.35 | 0.036 | 58 |
| (7) RF: Rectus femoris | Bi, hip flexor, knee extensor | 0.48 | 0.049 (h), 0.025 (k) | 12.5 |
| (8) BFL: Biceps femoris long | Bi, knee flexor, hip extensor | 0.46 | 0.054 (h), 0.049 (k) | 15.8 |
| (9) GC: Gastrocnemius | Bi, knee flexor, ankle plantar-flexor | 0.56 | 0.050 (k), 0.040 (a) | 30 |

or h to distinguish ankle, knee and hip joint moment arms, respectively, in bi-articular muscles). Flexor moment arms are negative reflecting the relationship between length change and rotational direction.

Passive muscular force is expressed by:

$$\mathbf{F}_p = \left[\mathbf{K}_p(\mathbf{l}_{eq} - \mathbf{l}) - \mathbf{B}_p\dot{\mathbf{l}} \right]_+ \quad (7)$$

where $[x]_+ = x$ if $x > 0$, $[x]_+ = 0$ if $x \leq 0$.

\mathbf{F}_p is passive tension vector; \mathbf{K}_p and \mathbf{B}_p represent respectively passive muscle stiffness and viscosity matrices; \mathbf{l}_{eq} is the muscle length vector at equilibrium; \mathbf{l} is actual muscle length vector. The positive brace means that each muscle is constrained to exert only contractile force. Active muscular force as a function of neural input to each muscle (\mathbf{act}) is represented by:

$$\mathbf{F}_a = \mathbf{K}_A(\mathbf{act})[\mathbf{l}(\mathbf{act}) - \mathbf{l}]_+ - \mathbf{B}_A(\mathbf{act})\dot{\mathbf{l}} \quad (8)$$

where $\mathbf{l}(\mathbf{act}) = \mathbf{l}_{eq} + \mathbf{act}$. \mathbf{F}_a is active tension vector; $\mathbf{K}_A(\mathbf{act})$ and $\mathbf{B}_A(\mathbf{act})$ represent respectively active muscle stiffness and viscosity matrices.

$$\begin{aligned} \mathbf{K}_A(\mathbf{act}) &= \mathbf{K}_{ACT}(\alpha[\mathbf{act}]_+ + \beta \min(\gamma[\mathbf{act}]_+, 1)) \\ \mathbf{B}_A(\mathbf{act}) &= \mathbf{B}_{ACT}(\alpha[\mathbf{act}]_+ + \beta \min(\gamma[\mathbf{act}]_+, 1)) \end{aligned} \quad (9)$$

where \mathbf{K}_{ACT} , and \mathbf{B}_{ACT} are constant matrices, and α, β , and γ are constant coefficients. For simulations, α, β , and γ are set to 0.11, 0.4, and 0.6 respectively. The coefficients are chosen such that Eq. 9 fits quasi-linearly the hill type muscle model [4].

When both passive and active tensions are applied together,

$$\mathbf{F}(\mathbf{l}, \dot{\mathbf{l}}, \mathbf{act}) = \left[\mathbf{F}_p(\mathbf{l}, \dot{\mathbf{l}}) + \mathbf{F}_a(\mathbf{l}, \dot{\mathbf{l}}, \mathbf{act}) \right]_+ \quad (10)$$

$$\mathbf{l} = \mathbf{l}_{eq} + \mathbf{A}(\Theta - \Theta_{eq}) \quad (11)$$

where Θ_{eq} is joint angle vector at equilibrium.

The muscle force formulations substantially follow those employed by [27]. As in [27], the formulations express the overall viscoelasticity of muscle-tendon system depending on the nerve activation.

The model views the anatomically redundant muscles of the trunk and legs as operating together as functional groups of mono- and bi-articular flexors and extensors. To determine the muscle stiffness and viscosity matrices, the following conditions are applied: (1) assuming that stiffness is proportional to physiological cross-sectional area (PCA) [2], the relative muscle stiffness scaling is given based on morphometric data in Table 1, (2) the effective intrinsic joint stiffness of the ankle during standing is about 90 Nm/rad [14], (3) for an infinitesimal deviation of movement, a simple relation between muscle stiffness and rotational stiffness can be expressed as $\mathbf{K}_r = \mathbf{A}^T \mathbf{K}_p \mathbf{A}$ where \mathbf{K}_r represents the rotational stiffness matrix. The

above three conditions enable to determine the absolute passive stiffness of each muscle given their relative scaling. For active muscle property, it was assumed that $\mathbf{K}_{ACT} = 2.5\mathbf{K}_p$ and $\mathbf{B}_{ACT} = 2.5\mathbf{B}_p$. This was considered based on human arm modeling where stiffness and damping ratio have been shown to increase up to 500 and 50%, respectively [28] with strong activation. Muscle viscosity was set at one-tenth the muscle stiffness as has been done in arm modeling [12].

The interaction between foot and ground is detected on the foot [35]. The ground contact information is expressed by R_t .

$$R_t = \begin{cases} 1 & \text{if } F_{gy}^T + F_{gy}^h > 0 \\ 0 & \text{if } F_{gy}^t + F_{gy}^h = 0 \end{cases} \quad (12)$$

For simplicity, detection is based on the total reaction force on the foot, which is a sum of reaction forces on the toe and heel. R_t is 1 when foot receives reaction force and 0 otherwise. The information of whether each leg is at either swing or stance phase is presumably sent to the cerebro-cerebellar system.

2.2 Neural control

2.2.1 Spino-locomotor

That humans have the existence of the central pattern generator (CPG) within the spinal cord has been supported by several studies [5, 9, 11]. In addition, muscle synergies are presumably encoded in the spinal cord [8, 37, 42]. Therefore, it is possible to consider that CPG is organized in such a network that implements distinct motor behaviors based on a few muscle synergies.

In [25], each of the principal waveforms is partitioned into five sequential control epochs: “loading” (LOA), “regulation” (REG), “thrust” (THR), “retraction” (RET) and “forward” (FOW) (see Fig. 2b). Each epoch is almost, but not precisely synchronous with each phase in a gait. No explicit pattern generation circuitry is proposed in this study. However, several potential implementations can be found in the literature [6, 15, 23, 38]. Effective muscular activation is afforded by a linear combination of five principal waveforms. The five phases were empirically determined: LOA corresponds to weight acceptance, REG to move of COM from behind to front of a contact point, THR to push the whole body forward, RET to contract a swing leg, and FOW to stretch a swing leg. In comparison to the previous model in [25], the control epoch FOW has an explicit pulse activation expressed by $u_{PG,5}(t)$ as below.

Five sequential pulse activations can be modeled in the form (Fig. 1a) of

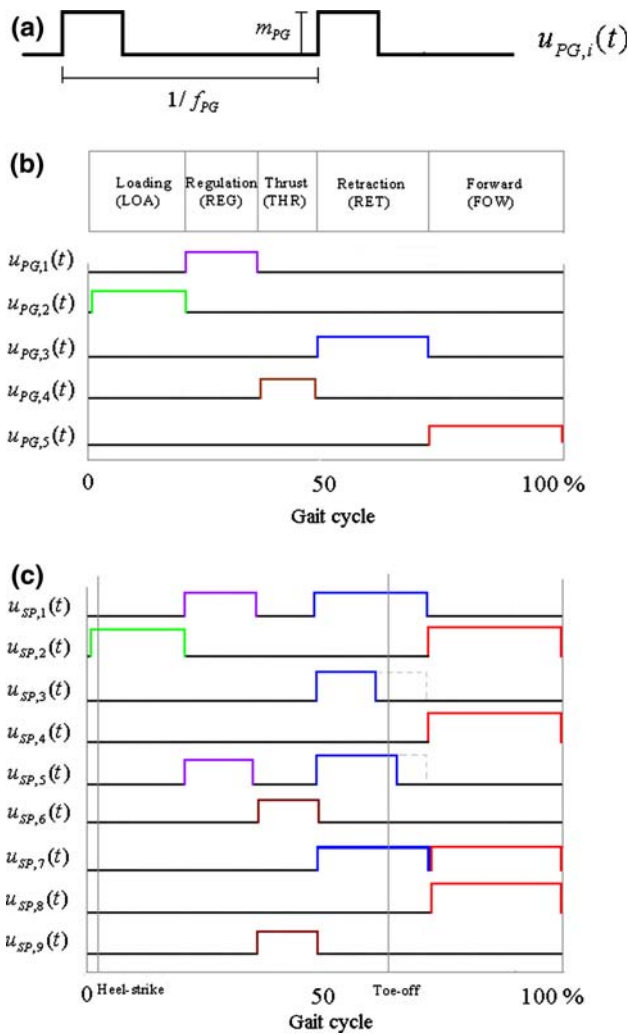


Fig. 1 **a** Distribution of the spino-locomotor signals, **b** five state pulse activations from the periodic pattern generator, **c** distribution of the spino-locomotor pulse signals to muscles: *dotted lines* indicate suppressed (inhibited) signals

$$u_{PG,i}(t) = m_{PG} \cdot 1[\cos(2\pi f_{PG}t - \phi_i) - h_i]_+, \quad i = 1, 2, 3, 4$$

and

$$u_{PG,5}(t) = m_{PG} \cdot 1[1 - u_{PG,1}(t) - u_{PG,2}(t) - u_{PG,3}(t) - u_{PG,4}(t)]_+ \tag{13}$$

where $1[x]_+ = \begin{cases} 1 & \text{where } x > 0 \\ 0 & \text{where } x \leq 0 \end{cases}$. f_{PG} determines the pattern frequency, m_{PG} is a magnification factor, ϕ_i is the phase shift, and h_i activity discharge threshold of the i th spinal command signal $u_{PG,i}(t)$. The appropriate values used for ϕ_i and h_i in simulation are empirically chosen as in Table 2 (Appendix C). The last pulse is modeled to activate when others are all suppressed.

It is noted [22] that during each of these subphases the muscular EMG principal patterns are fairly unique, and consistent across movement speeds, changing only in

duration and intensity. It is therefore plausible that these five phases are driven by the equivalent of a five-state pattern generator as shown in Fig. 1b that can cycle with a range of frequencies. Although a priori it is not necessary that the relative durations of each subphase remain fixed, this is the simplest assumption.

It is proposed that pulse commands $\mathbf{u}_{PG} = [u_{PG,1} \ u_{PG,2} \ u_{PG,3} \ u_{PG,4} \ u_{PG,5}]^T$ are distributed to both mono- and bi-articular muscles through a spino-locomotor network represented by the matrix \mathbf{W}_{PG} . $u_{PG,5}$ affects mainly hip extension and knee stretch during the swing phase through \mathbf{W}_{PG} . For realization of a nominal walking behavior, this may not be necessary as in [25]. However, modulated behaviors requires more robust swing motion smoothly transitioned to the ground contact. Allowing muscular activation during the swing phase seems useful in the perspectives. The rhythmic patterns to a leg are respectively 180 degrees phase different from those to the other leg to realize walking motions.

$$\mathbf{u}_{SP} = \mathbf{W}_{PG}\mathbf{u}_{PG} \tag{14}$$

The spinal activations $u_{SP,j}(t)$ are determined for each muscle as in Fig. 1c. The number in the subscript j indicates the corresponding muscle in Table 1.

It is proposed that peripheral spinal reflex helps improve walking patterns. One potential neural circuit called pre-synaptic inhibition [3, 35, 36] is embedded to modify principal spinal activations. A tonic excitation $\theta_{th,jo}$ ($jo = a, k, h$: ankle, knee, hip respectively) represents a descending signal which inhibits the proprioceptive afferent θ_{jo} . Once $\theta_{th,jo}$ is superseded by θ_{jo} , the interneuron is activated and the motor neuron activity is suppressed. Such a mechanism can suppress pulse activities in early FOW as in Fig. 1c to prevent excessive leg retraction. This mechanism is useful to implement the right timing between knee and ankle stretching motions not to touch the ground during swing phase. The reflex action is modeled as:

$$\mathbf{u}_{reflex}(t) = -\mathbf{W}_{reflex} \cdot 1[\hat{\boldsymbol{\theta}}_{pr} - \boldsymbol{\theta}_{th}]_+ \tag{15}$$

where $\hat{\boldsymbol{\theta}}_{pr} = [\theta_a(t - T_{pr,a}) \ \theta_k(t - T_{pr,k}) \ \theta_h(t - T_{pr,h})]^T$, and $\boldsymbol{\theta}_{th} = [\theta_{th,a} \ \theta_{th,k} \ \theta_{th,h}]^T$, and \mathbf{W}_{reflex} is a matrix that distributes joint-related signals to muscles via the element vector \mathbf{u}_{reflex} , and $T_{pr} = [T_{pr,a} \ T_{pr,k} \ T_{pr,h}]^T$ that represents neural transmission delays from muscle to the spinal cord.

2.2.2 Cerebro-cerebellar (supraspinal) long-loop feedback system

2.2.2.1 Hypothetical cerebellar computation

Ito [19] proposed that cerebellar processing is performed by functional corticonuclear microcomplexes. Under the

framework, the cerebellum may compute proportional scaling, integration, and differentiation [24, 29, 30]. Figure 2a illustrates cerebellar neural circuitry in the lateral cerebellum. The deep cerebellar nuclei convey the output signal $u_{cb}(t)$. The cerebellar input signal $x_{cb}(t)$ directly excites the deep cerebellar nuclei and the Purkinje cell through the ascending segment. Then, the Purkinje cell inhibits the deep cerebellar nuclei. Therefore, there are two neural pathways between the input and output. The neural activities through the pathways are modeled as follows [24, 29, 30]:

$$\lambda_1 x_{cb}(t) - \lambda_2 x_{cb}(t - \Delta) = \lambda_1 (x_{cb}(t) - x_{cb}(t - \Delta)) + (\lambda_1 - \lambda_2) x_{cb}(t - \Delta) \tag{16}$$

where Δ is neural transmission delay and λ_1, λ_2 are coefficients representing intensity of activity.

The first term above on the right hand side is interpreted as differential operation in the continuous domain, and the second as proportional operation. Therefore, the input and output signals of the cerebellar gainscheduling circuitry are in the relation of

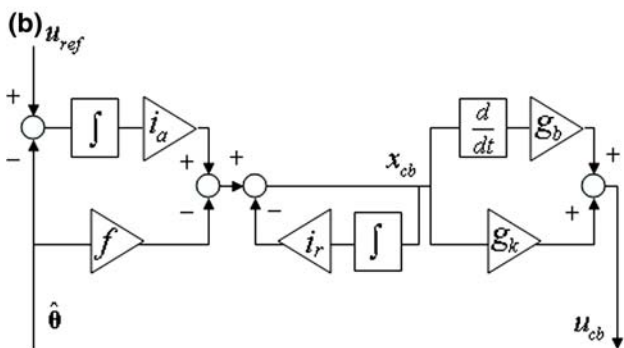
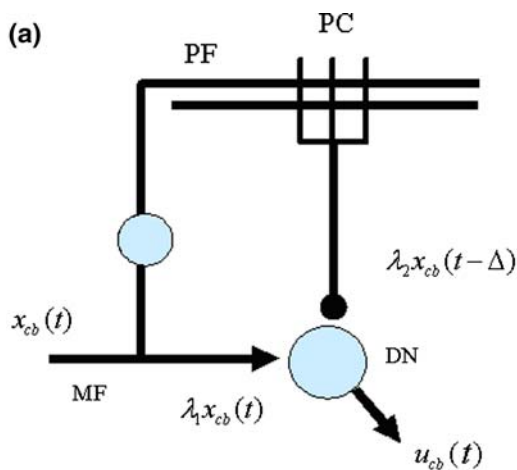


Fig. 2 a Cerebellar computation model; *PF* parallel fibers, *PC* Purkinje cell, *MF* mossy fibers, *DN* deep nuclei, **b** the cerebro-cerebellar system model

$$u_{cb}(t) = g_b \dot{x}_{cb}(t) + g_k x_{cb}(t) \tag{17}$$

where g_b represents the cerebellar derivative gain, and g_k the cerebellar proportional gain.

2.2.2.2 Supraspinal system The cerebro-cerebellar (supraspinal) system is modified from [24] as in Fig. 2b. i_a represents the scaling of the signal related to hypothesized sensorimotor cortical integrator [26]. f affects the relative balance of cortical and cerebellar circuitries. The activity related to a reverberating circuit between u_{cb} and x_{cb} is implemented by integration [29][30]. i_r is the scaling of the integral signal projected to cerebral cortex in a recurrent feedback manner [30]. Hypothetically, the signal on the projection pathway is comparable with “efference-copy” discharge.

For generation of normal walking, the cerebro-cerebellar control channel is modeled. The channel is presumably concerned with tracking the commanded position of the body’s COM as specified by a tonic reference signal. This signal indicates the relative position of the COM from a ground contact point. During simulated walking, it remains constant to be 25 cm ($u_{ref} = 0.25$). A COM position relative to the stance foot is linearly estimated as:

$$\begin{aligned} \hat{x}_{com} &= \frac{m_1}{(m_1 + m_2 + m_3)} r_1 \sin \theta_a(t - T_{spr,a}) \\ &+ \frac{m_2}{(m_1 + m_2 + m_3)} (l_1 \sin \theta_a(t - T_{spr,a}) \\ &+ r_2 \sin(\theta_a(t - T_{spr,a}) + \theta_k(t - T_{spr,k})) \\ &+ \frac{m_3}{(m_1 + m_2 + m_3)} (l_1 \sin \theta_a(t - T_{spr,a}) \\ &+ l_2 \sin(\theta_a(t - T_{spr,a}) + \theta_k(t - T_{spr,k})) \\ &+ r_3 \sin(\theta_a(t - T_{spr,a}) + \theta_k(t - T_{spr,k}) + \theta_h(t - T_{spr,h})) \\ &\approx \frac{(m_1 r_1 + m_2 (l_1 + r_2) + m_3 (l_1 + l_2 + r_3))}{(m_1 + m_2 + m_3)} \\ &\theta_a(t - T_{spr,a}) + \frac{(m_2 r_2 + m_3 l_2)}{(m_1 + m_2 + m_3)} \theta_k(t - T_{spr,k}) \\ &+ \frac{m_3 r_3}{(m_1 + m_2 + m_3)} \theta_h(t - T_{spr,h}) \end{aligned} \tag{18}$$

where $\theta_a, \theta_k,$ and θ_h are ankle, knee, and hip joint angles of supporting leg; $m_i, r_i,$ and l_i are respectively mass, length between COM and lower end, and length of each body segment ($i = 1$: shank, $i = 2$: thigh, $i = 3$: trunk–head segment).

$\mathbf{T}_{spr} = [T_{spr,a} \ T_{spr,k} \ T_{spr,h}]^T$ are the afferent signal transmission delays including spinal and peripheral components from limb joint to head. The estimate neglects the contributions of the swing leg. The determinant of which leg is in stance or in swing is sensed signal of ground contact (see Eq. 12).

Therefore,

$$\hat{x}_{\text{com}} = p_1\theta_a(t - T_{\text{spr,a}}) + p_2\theta_k(t - T_{\text{spr,k}}) + p_3\theta_h(t - T_{\text{spr,h}}) = \mathbf{p}^T\hat{\boldsymbol{\theta}} \tag{19}$$

where $\mathbf{p} = [p_1 \ p_2 \ p_3]^T$ are constants, and the scaling factors p_i were consistent with coefficients in Eq. 18, and $\hat{\boldsymbol{\theta}} = [\theta_a(t - T_{\text{spr,a}}) \ \theta_k(t - T_{\text{spr,k}}) \ \theta_h(t - T_{\text{spr,h}})]^T$.

It is known that the interpositus nucleus projects to the cortex and could be involved in cerebro-cerebellar coordination. It may be possible to interpret that output from the COM-related channel is comparable with the interpositus. The cerebral cortex is presumably the spot where population vector \mathbf{p} is implemented. In sensorimotor cortical area 3a, the spatial extend of pyramidal cell association collaterals approximately construct a columnar assembly. It could be expected that each column contains a specific feature presentation of sensory information [18]. The specific presentation can be described by a weighted linear combination of sensory information, which is a form of the inner product of a population vector \mathbf{p} and a vector of sensory information as in Eq. 19 [16]. Hypothetically, a columnar activity is represented by a unit population vector $\hat{\mathbf{p}}$ parallel to \mathbf{p} .

$$\mathbf{p} = k\hat{\mathbf{p}} \tag{20}$$

where k is a scalar that represents the intensity of neural activity.

When x_{cb} is the input, u_{cb} is the output in Fig. 2b, we can describe cerebellar control as:

$$u_{\text{cb}} = (g_k + g_b d(\cdot)/dt)x_{\text{cb}}, \tag{21}$$

and

$$x_{\text{cb}} = L^{-1} \left\{ (s + i_r)^{-1} \left(i_a \left(u_{\text{ref}} - \mathbf{p}^T\hat{\boldsymbol{\theta}}(s) \right) - sf\mathbf{p}^T\hat{\boldsymbol{\theta}}(s) \right) \right\} \tag{22}$$

where s is the Laplace variable, L^{-1} is the inverse Laplace transform, g_k and g_b are, respectively, proportional and derivative control gains, $d(\cdot)/dt$ is the differentiation operator.

For simulation of normal walking, it was found empirically that $g_b = 0$. The g_b is used to scale differential (high frequency) signals attributed to lateral cerebellum whose output is through the dentate nuclei. While it has been noted that there is apparently a complete somatotopic body representation within the dentate [41], the dentate is generally seen to be less active with truncal and leg movement rather than with arm and hand movements. This is also in comparison with the activities of the interpositus and fastigial nuclei that are strongly involved in leg movement control [1, 32] and presumably represented as g_k in the model.

Finally,

$$\mathbf{u}_d = R_t \mathbf{W}_C u_{\text{cb}} \tag{23}$$

where \mathbf{W}_C is a distribution matrix in either cerebral cortical area 4 or in the spinal cord.

R_t from Eq. 12 indicates the ground contact. In this model, the descending command from the cerebro-cerebellar control is conveyed to the muscles of the stance leg, and activates the muscles in order to move the body's COM to a desired position with respect to the stance leg. The muscular activation distribution is determined by \mathbf{W}_C . Because the left and right legs keep switching to be the stance leg, catching up a desired position relative to each stance leg drives a forward movement.

The vestibular system, presumably through the vestibulo-spinal reflex, concerns maintaining the trunk-head segment vertical. The pitch angle of the trunk-head segment is represented as θ_{tr} and therefore the reference of its vertical position is set to be $\theta_{\text{tr,ref}} = 0$. The estimate of θ_{tr} is notated by $\hat{\theta}_{\text{tr}}$. In the case of non-horizontal surfaces, the trunk-head segment pitch estimate is presumably adjusted on the basis of or replaced by further visual and/or vestibular input. However, this issue is not examined here.

The vestibulo-spinal reflex is simply modeled as:

$$\mathbf{u}_{\text{ves}} = \mathbf{W}_{\text{ves}} \left(k_p (\theta_{\text{tr,ref}} - \hat{\theta}_{\text{tr}}) - b_p \dot{\hat{\theta}}_{\text{tr}} \right) \tag{24}$$

where \mathbf{W}_{ves} is a distribution vector, and k_p and b_p are respectively proportional and derivative gains.

In summary, the descending command (\mathbf{u}_{desc}) at the level of the spinal cord resulting from the supraspinal system can be represented as:

$$\mathbf{u}_{\text{desc}} = \mathbf{u}_d(\mathbf{t} - \mathbf{T}_{\text{sp}}) + \mathbf{u}_{\text{ves}}(\mathbf{t} - \mathbf{T}_{\text{sp}}) \tag{25}$$

where \mathbf{T}_{sp} represents the neural transmission delays from the supraspinal system to the spinal cord.

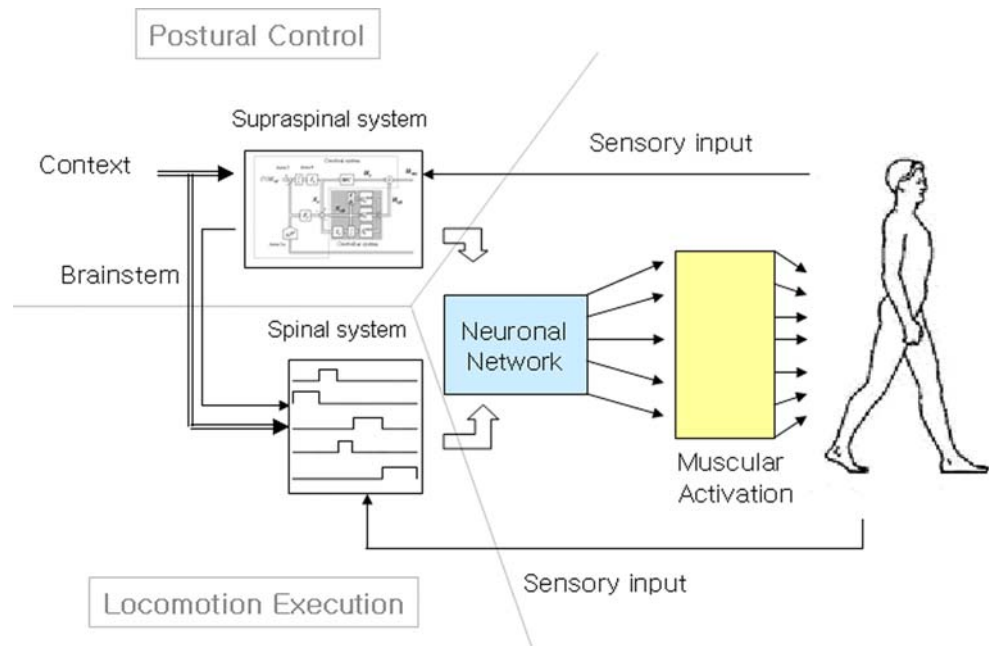
2.2.3 Summary of neural control model

Alpha motor neuronal output \mathbf{u}_α is represented by a nine component vector. From Eqs. 14, 15 and 25,

$$\mathbf{u}_\alpha = \mathbf{u}_{\text{desc}} + \mathbf{u}_{\text{SP}} + \mathbf{u}_{\text{reflex}} \tag{26}$$

The major feature of the model of sagittal control of bipedal walking (SCBW) is the functional decoupling over the hierarchical neural control circuits even though the functions are not perfectly separate. The spino-locomotor system executes gaits, and supraspinal system controls dynamic postural balance (Fig. 3). Segmental reflex in the level of spinal cord helps regulate interlimb movement. The supraspinal control relevant to the location of COM plays a main role as the postural control of the lower limb,

Fig. 3 Hierarchical neural control of walking



and the vestibulospinal control to truncal verticality as that of the upper limb. Each neural system performs each role while an integrated system achieves a stable walking behavior. Such decoupling scheme makes it possible to avoid the overall complicated recomputation of motor program when the body responds to environment or elicit a new behavior. A simple adjustment of the relevant local neural system may enable simply the achievement of behavioral adaptation. The paper intends to demonstrate computationally the scheme’s potential. A linear superposition is a simple realization of the adjustment. If the mechanism were implemented in vivo, it would be quite powerful in terms of behavioral modification or adaptation.

2.2.4 Implementation of voluntary modulation

The neural network in a fully trained person is expected to reserve the principal pulse patterns for locomotion and have no difficulty in generation of nominal walking. Once nominal walking patterns are achieved, voluntary modulation via superposition would allow for the generation of more complex behaviors. For example, if any context intends to modify kinematic or kinetic patterns corresponding to voluntary modulation, e.g., further excursion of a swing leg to step over an obstacle on the ground during locomotion, CNS may generate additional neural signals which were not activated during nominal walking. The new neural signals will affect some specific muscular activations so as to produce appropriate kinematic or kinetic patterns, which could not be realized without the additional muscular activations. For computational modeling, a

possible representation of the new signal activation could be simply additional pulse-like commands like those assumed to be generated by the spino-locomotor. This paper aims to realize modulated behaviors during walking based on the simple assumption.

An additional pulse activation $u_p(t)$ passes through neural network \mathbf{W}_v to be

$$\mathbf{u}_v(t) = \mathbf{W}_v u_p(t - T_{sp}) \tag{27}$$

Then it is superposed to neural pattern generator network to implement behavior response to voluntary perturbation as follows.

$$\mathbf{u}'_\alpha(\mathbf{t}) = \mathbf{u}_\alpha(\mathbf{t}) + \mathbf{W}_v \mathbf{u}_v(\mathbf{t}) = \mathbf{u}_{desc}(\mathbf{t}) + \mathbf{u}_{reflex}(\mathbf{t}) + \mathbf{u}_{sp}(\mathbf{t}) + \mathbf{u}_v(\mathbf{t}) \tag{28}$$

It should be notified that the overall activation from the spinal pattern generator and the additional pulse are still under the effect of the segmental spinal reflex (Eq. 15). If a joint angle is over its threshold value, the activation is suppressed. The cerebro-cerebellar feedback control remains unchanged.

Ivanenko et al. [22] analyzed voluntary modulations of nominal gait using the principal component analysis and found that their muscular activations can be decomposed. In comparison with nominal walking, voluntary modulation included an additional principal factor in EMG waveforms, and similar other factors. Even though the investigation does not prove the plausibility of an additional pulse-like command in CNS, the proposed commands scheme is theoretically attractive due to its simplicity. Moreover, the scheme conserves the property of superposition. Even with the modification, the primary functional performance of

each neural system still remains consistent with that during nominal walking. The SCBW model proposes that the compound motor primitives of simple locomotor pulse patterns and voluntary activations may be sufficient to generate voluntary modulation during walking.

2.2.5 Model evaluation

The SCBW model is evaluated first in terms of its steady state walking features. Then, the voluntary perturbation of normal walking is tested with the SCBW model: stepping over an obstacle, and kicking a ball during walking. These voluntary tasks are chosen because the tasks have been experimentally observed [21]. In addition, a different style of walking, i.e., walking with trunk bent forward, is tested. The bent walking is also experimentally observed [17]. These test examples are used to evaluate the feasibility and benefits of decoupling between neural systems, and those of superposition of neural network. During the simulations, all model parameters were held fixed unless explicitly stated otherwise. No optimization of performance is intended because the goals of this paper are the potential explanation of the principles behind the system and its performance—not achieving maximal performance.

3 Results

3.1 Generation of normal walking pattern

The SCBW model generates normal human-like walking motion at natural speed of about 1.2 m/s (Fig. 4). After an initial transient response, body kinematics converges closely to a consistent normal walking pattern. Each joint constructs a limit cycle.

Kinematic behavior of steady walking generated by the model is described in the stick plot (Fig. 4a) and in the phase plot (Fig. 4b). Each joint motion constructs a limit cycle achieving steady state walking motions. The simulated gait pattern is compared with the typical pattern of human walking in joint trajectories (Fig. 4c). Typical behavioral features such as a push off valley at ankle trajectory, small knee bending motion at transition from swing to stance and large knee bending at transition from stance to swing, and monotonic sway motion at hip in the anterior–posterior direction, are realized in simulation.

The pulse epochs in spinal pattern generator are empirically determined to achieve stable normal walking patterns under the assumption of five sequential control epochs explained previously. Then, the simulated EMG (\sim muscle command act) is compared with observations from [21] (Fig. 4d). Activations of GM, GC, BFS, BFL and

SO are reasonably close to observations, and activations of IP, TA, RF either include extra pulse or phase shift. This may implicate some discrepancy between the model and real humans such as variability in how a movement is performed. Lateral pelvic tilt and its effect of the resulting body kinematics is likely to play a role in this discrepancy. The model describes sagittal motion not lateral motion whose amplitude is actually about 5 cm in real humans [19]. The side-to-side movement locates COM near the midline at heel strike and over the supporting leg during stance phase. This results in adduction of the leg during stance and abduction of the leg during swing. Therefore, the model may require extra activation, probably in tensor fasciae latae, to have the same effect as lateral motion does. At transition from swing to stance, simulated activations of VA, RF trigger early to move an upper body forward to strike heel on time. During midstance, IP and TA have extra pulse to move the upper body forward to obtain a right posture for swing.

Figure 4e demonstrates simulated ground reaction force profiles. Horizontal force profile is biphasic, and vertical force profile includes two peaks, which are qualitatively comparable with typical patterns from empirical observation [43].

3.2 Generation of walking patterns with voluntary perturbation

3.2.1 Kicking motion during walking

The SCBW model simulates a kicking task. A human walks at natural speed and kicks a stationary ball in the locomotion path with the right leg. The force of the kick is fixed to be 90 N according to experiment [21], and the force is decomposed into horizontal and vertical as follows.

$$F_x = -90 \cos(30^\circ), \quad F_y = -90 \sin(30^\circ).$$

For simulation, the impulsive force is applied on the right foot at instant of kicking for 50 ms.

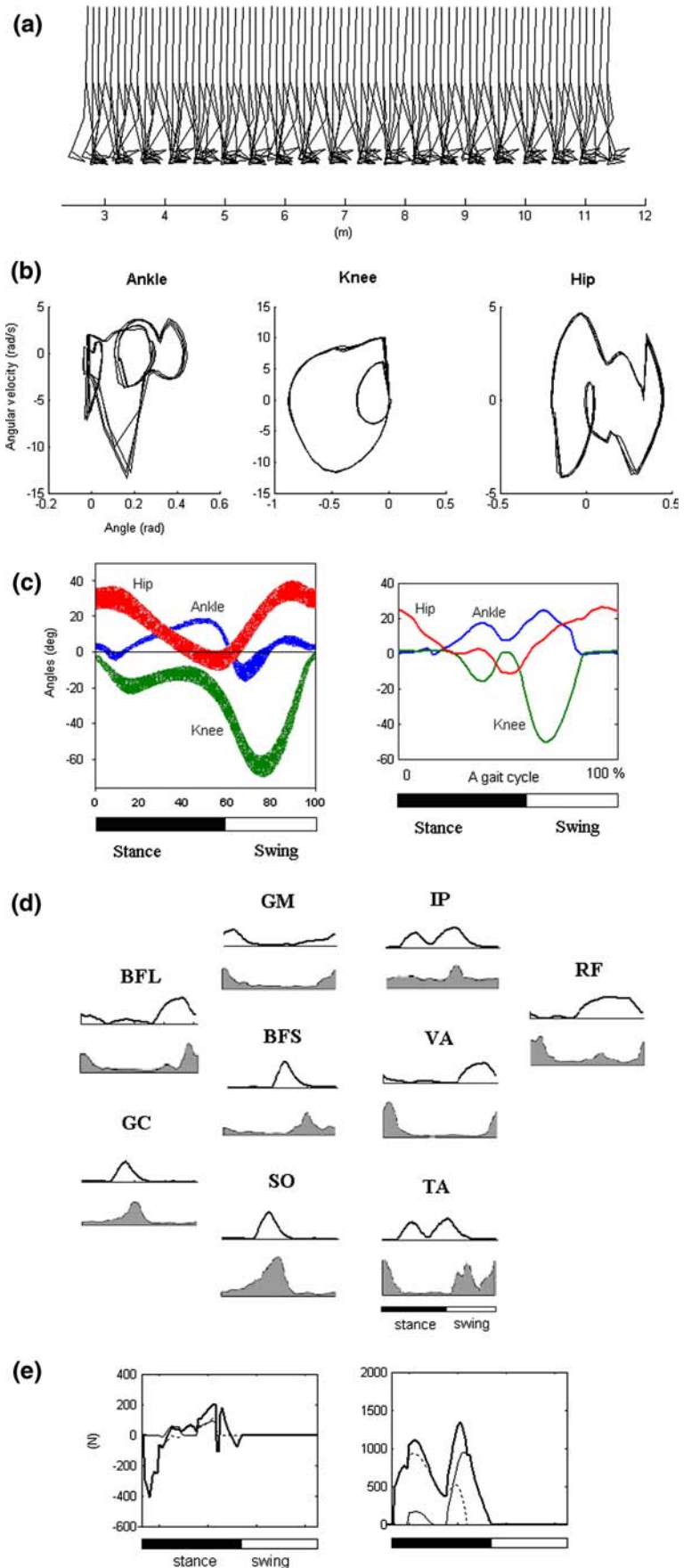
An additional pulse of the voluntary activation for kicking is applied before reaching the ball during swing phase (Fig. 5). To compensate for the impact of the kick and maintain stable posture, the pulse is distributed over the muscles in both legs.

$$\text{For the right (swing) leg, } \mathbf{W}_V \\ = [0.2 \ 0 \ 0 \ 0 \ 0.2 \ 0 \ 0 \ 0 \ 0]^T$$

$$\text{For the left (stance) leg, } \mathbf{W}_V \\ = [0 \ 0 \ 0.4 \ 0 \ 0 \ 0 \ 0 \ 0 \ 0]^T.$$

where each element of the 9×1 vector \mathbf{W}_V propagates additional activation to corresponding muscle. i th muscle in Table 1 corresponds to i th element in \mathbf{W}_V .

Fig. 4 Normal walking simulation: **a** stick plot of motion, **b** joint phase-plane behaviors, **c** comparison of observed (*left*) and simulated (*right*) joint trajectories during a gait cycle: the experimental data is adapted from CGA normative gait database (guardian.curtin.edu.au/cga/data/index.html), **d** simulated (*upper trace*) and observed EMG patterns (*bottom filled gray*) during a gait cycle; data is adapted from [21], **e** ground reaction force profiles: *left* horizontal, and *right* vertical



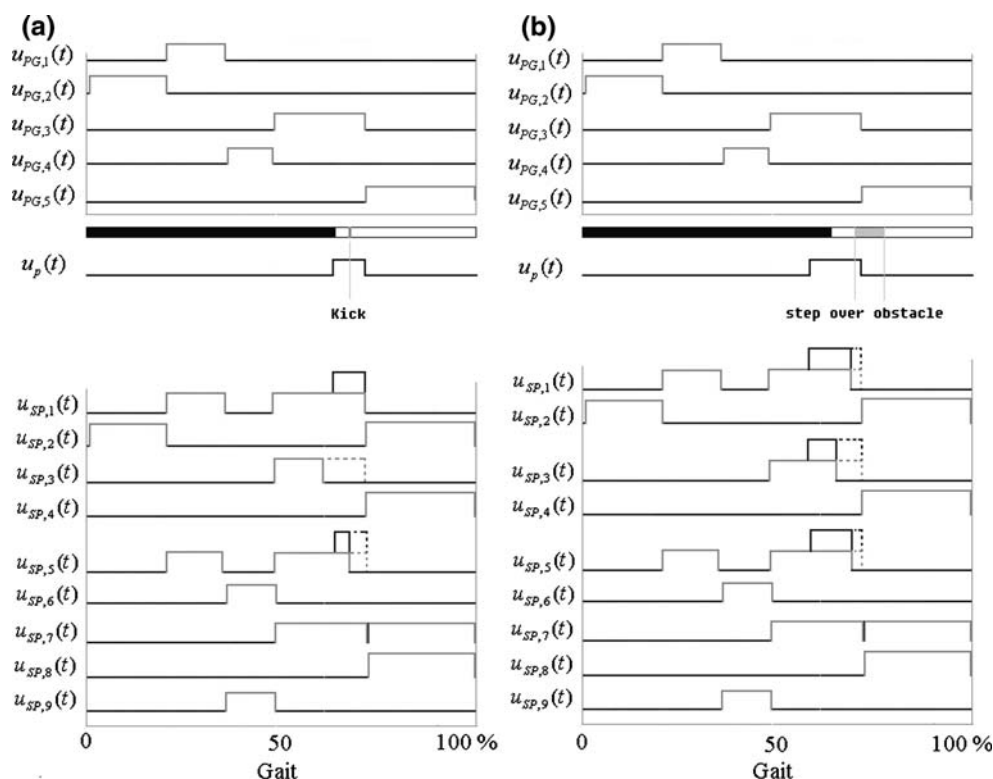


Fig. 5 Decomposed spino-locomotor signals. *Top* neural signals from the pattern generator plus an additional voluntary signal. *Bottom* spinally generated command to muscles (in right leg) for kicking a

ball (a), and stepping over an obstacle (b). Bar indicates gait phase (black stance, white swing)

W_V scales and distributes the additional pulse to adjust appropriate muscular activations.

3.2.2 Stepping over an obstacle during walking

As in [20], the simulation describes that a human walks at natural speed and step over an obstacle with the right leg. A new pulse of the voluntary activation for stepping is applied at the timing of swing just in front of an obstacle (Fig. 5). The pulse activation is transferred to each muscle via a distribution matrix. Joint angles of swing leg should have large excursions to lift up the foot over the obstacle while stance leg supports the whole body robustly and moves the swing leg quickly to the ground. The pulse activation affects on muscles in both legs.

For the right (swing) leg, W_V

$$= [0.7 \ 0 \ 0.55 \ 0 \ 0.3 \ 0 \ 0 \ 0 \ 0]^T$$

For the left (stance) leg, W_V

$$= [0.2 \ 0 \ 0 \ 0 \ 0.3 \ 0 \ 0 \ 0 \ 0]^T.$$

In addition, the value of $\theta_{th,jo}$ in Eq. 15 is temporally adjusted to allow large excursion of joint angles in swing leg. As mentioned earlier, $\theta_{th,jo}$ may be the descending

tonic excitation which includes the command from supraspinal control. The cerebrum presumably regulates joint excursion by the descending signal. Therefore, $\theta_{th,jo}$ conveys a new value only for joints in swing leg during the voluntary behavior and recovers the old for normal walking.

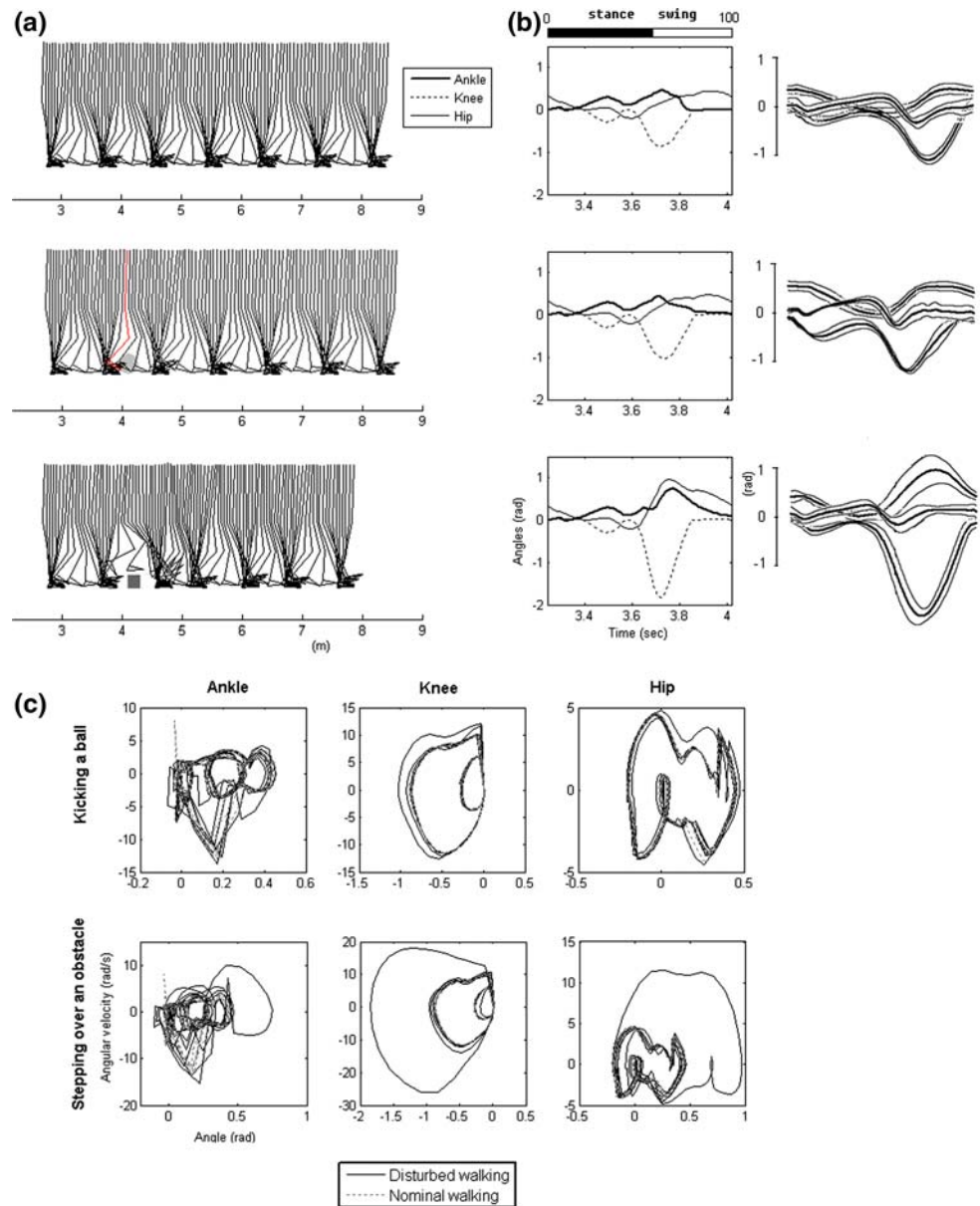
$$\theta_{th,jo} = \begin{cases} 0.35 : jo = a, \\ -0.35 : jo = k, \\ 0.55 : jo = h \end{cases} \text{ for normal walking,}$$

$$\theta_{th,jo} = \begin{cases} 0.35 : jo = a, \\ -0.65 : jo = k, \\ 0.55 : jo = h \end{cases}$$

only while the voluntary pulse $u_p(t)$ activates.

Voluntary perturbations are applied after the model achieves closely steady walking patterns. The extra force reaction of the kick can affect the kinematic patterns. However, experimental results show that the kinematic patterns of the kick are nearly identical to those of normal walking [21]. Figure 6 demonstrates that simulation abides with it. As in Fig. 6b, simulated joint trajectories are compared with observed ones for each case. Phase plane shows kick motion does not deviate much from normal

Fig. 6 (a) Stick plots of kinematics (right leg only for clarity), (b: left) simulated and (b: right) observed joint trajectories (adapted from [21]) of a gait cycle during voluntary perturbations, (c) phase planes in comparison with normal walking



walking patterns (Fig. 6c). Modified activation by an additional pulse is kinetically to compensate for the impact of the kick. When a human steps over an obstacle in their pathway, the kinematics are obviously quite modified from those of normal walking. The knee and hip angles excure largely to shorten the length of lower limb in swing phase (Fig. 6b, c). In this case, an additional pulse modifies muscular activations to change angular motions kinematically. Stick plots in Fig. 6a demonstrate clearly overall body movements of normal walking (top), kicking (middle), and stepping (bottom). Both kicking and stepping simulations demonstrate behavioral characteristics qualitatively consistent with experimental observations studied in [21].

3.2.3 Walking with trunk bent forward

To implement simulation of the forward bent locomotion, The values of two parameters, $\theta_{tr,ref}$ and \mathbf{W}_{PG} , are changed. The change of $\theta_{tr,ref}$ adjusts the desired position of trunk. To walk with bent trunk, cerebral cortex has presumably to command a bent desired position of trunk. The mechanism to process the change of \mathbf{W}_{PG} is controversial. There may exist a set of spinal pattern generation network for the bent locomotion. The other possibility is a set of pulse activations is superimposed on the spinal pattern generation network for the normal locomotion. The latter is an extension version of the superposition scheme of an additional pulse. A set of voluntary pulses could activate

instead of an additional pulse. Further investigation will be required to find if either hypothesis is true or if any other mechanism is plausible. Initial positional condition for simulation is modified to pose forward bent.

After some steps, walking converges to a steady motion with a steady walking speed of 1.5 m/s (Fig. 7).

When human walks with their trunk bent forward, the body's COM is located further forward in comparison to normal walking. Therefore, its location is closer to the front boundary of feasible support area, which means that a body would fall forward when stable posture is lost. To prevent the forward falling, the hip is displaced backwards compared with its position of normal walking. The hip location helps keep COM within the stable support area. Also, the stance leg is stretched and forward propulsion at toe-off is reduced because the upper body is already forward.

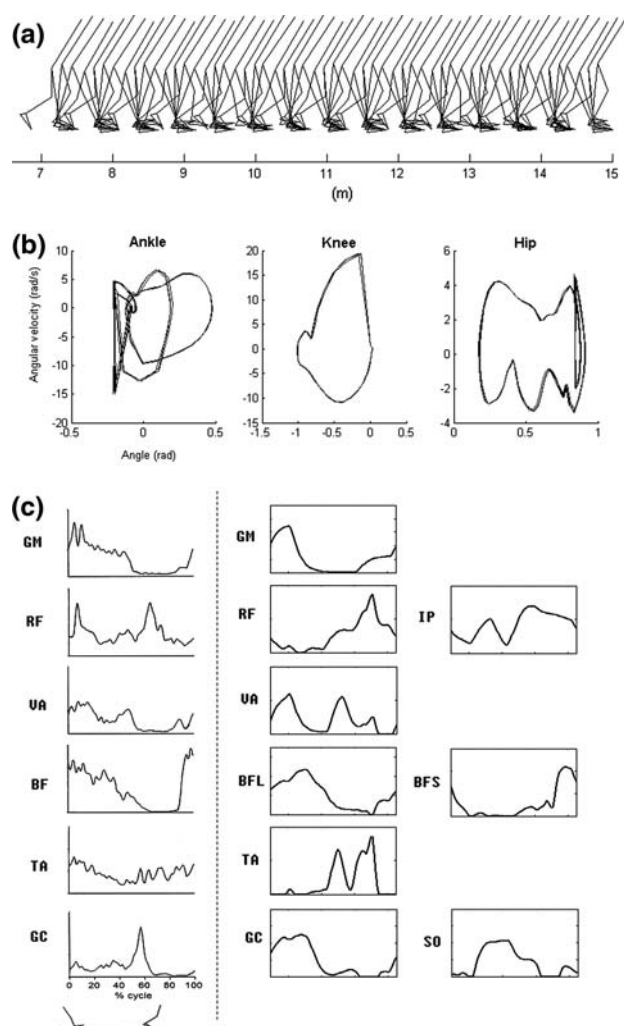


Fig. 7 Trunk bent walking simulation: (a) Stick plot of motion, (b) joint phase-plane behaviors, (c) observed (left to dotted vertical line) and simulated (right) EMG patterns; data is adapted from [17]

As mentioned earlier, no optimization is performed to improve upon model performance. Therefore, perfect match with experimental data is not expected, but the comparison helps demonstrate the feasibility and effectiveness of the proposed control mechanism. EMG profiles provide useful information. Figure 7c shows observed and simulated EMG patterns. Mono- or bi-articular muscles presumably with the same role are compared together. The patterns are roughly consistent while plantarflexor and dorsiflexor are not comparable with experimental data. With no intention of optimization, it is impressive that the SCBW model can implement the bent walking from the normal walking by a simple tuning of $\theta_{tr,ref}$ and \mathbf{W}_{PG} .

4 Discussion

It has been shown experimentally that electrical stimulation of the posterior structures of the lumbar spinal cord can induce patterned, locomotor-like activity [9]. Importantly, focal stimulation elicits simultaneous rhythmic EMG activities in muscles at different joints in the lower limb. This suggests that neural oscillators are not joint specific and is highly consistent with the synergies used. A synergy is in principle a consistent pattern in a set of muscular activities that may perhaps be modulated or shifted by the same factor. The concept of the synergy is proposed as an efficient solution of the dimensional reduction of the motor program. The CNS may simplify the control problem by utilizing a finite set of the synergies instead of an infinite set of muscle patterns. The usefulness of the idea has already been tested by applications to biologically inspired robot [31].

Periodic patterns from the five-state pattern generator are principally the locomotion synergies that constitute the forward command to the alpha motor neuron pool and the corresponding muscles. The linear combination of the simple pulses allows easily the composition of synergies. The combination of the state pattern generator and the concept of the synergy provide a framework for simplifying motor control of locomotion. The SCBW demonstrates that kinematic control is sufficient for gait generation with no detailed dynamic information.

SCBW model proposes that body control is divided between command channels significantly decoupled within the hierarchical neural structure even though the command effects are not perfectly separate. The spinal pattern generator provides the primary control of gait motion while the supraspinal system exerts major control over postural regulation. Spinal segmental reflex helps modulate inter-limb movement. The cerebro-cerebellar channel that controls the location of COM exerts its greatest effect at the

ankle. Control of trunk verticality is accomplished primarily at the hip. A change in trunk angle does affect COM position, but only weakly relative to that in ankle angle. When the body responds to environment or a new behavior is elicited, the effectively decoupled control makes it possible to learn the new behavior as a modification of a previously learned behavior rather than as a completely new behavior. In such control system, a local adjustment allowed for different behaviors to be simply elicited, i.e., different walking speeds by tuning parameters in spinal pattern generator only [35]. For implementation of forward bent walking, the tuning of desired trunk position without concerning the location of COM was effective. It was demonstrated here that the substantial decoupling of control may allow behavior modification by a simple superposition scheme.

This paper has identified arguably a potentially efficient way in which human balance and locomotor behaviors naturally decouple, which could be a motor behavioral basis. And this paper proposes that if simple control engages these natural dimensions with simple, low-dimensional feedforward and feedback processing, that sturdy building blocks become available for a wealth of behaviors that can continue to be controlled by simple commands with superposition. This may provide a simple adaptive scheme of behaviors. It is noteworthy that a linear combination of forward commands in the SCBW model does not only function partially as an approximated desired trajectory, but also tune continuously the control gains, i.e., muscle stiffness and viscosity. This provides a further flexible controllability over various motion generations. For example, the feature empowers the muscle to regulate different motion speeds even for motions in a same path. Also, the gain control is related to energy efficiency as well as fast motion control.

Appendix A: Anthropometry used to model a human body

The length of each segment is represented with respect to the total body’s height h_t (=180 cm) and mass m_t (=80 kg) based on [41]. trunk, thigh, shank, and foot masses are respectively $0.678 m_t$, $0.1 m_t$, $0.047 m_t$, and $0.015 m_t$; their moments of inertia are respectively $0.031 m_t h_t^2$, $6.262 \times 10^{-4} m_t h_t^2$, $2.566 \times 10^{-4} m_t h_t^2$, and $4.976 \times 10^{-6} m_t h_t^2$; their lengths are respectively $0.47 h_t$, $0.245 h_t$, and $0.246 h_t$; their COM distances from lower end are respectively $0.235 h_t$, $0.1389 h_t$, and $0.1395 h_t$; foot is modeled as a triangle with height $0.039 h_t$ and length $0.152 h_t$; foot COM is located at $0.0195 h_t$ high from bottom and $0.0304 h_t$ ahead from heel.

Appendix B: Foot interaction with the ground

The vertical ground reaction force is modeled by:

$$F_{gy}^i = (K_{gy}(f_{gy}(x^i) - y^i) - B_{gy}\dot{y}^i) \cdot 1[f_{gy}(x^i) - y^i, 0]_+ \quad (29)$$

where (x^i, y^i) indicates the positions of either heel or toe with $i = \text{heel, toe}$. $f_{gy}(x^i)$ represents the ground profile as a function of x^i .

If the toe or heel reaches zero horizontal velocity, the horizontal reaction force is modeled by a spring and damper system as long as the horizontal reaction force is smaller than the maximal friction force.

$$F_{gx}^i = (K_{gx}(x_o^i - x^i) - B_{gx}\dot{x}^i) \cdot 1[f_{gy}(x^i) - y^i, 0]_+ \text{ if } |F_{gx}^i| \leq |\mu_s F_{gy}^i|, \quad i = \text{heel, toe} \quad (30)$$

where x_o^i is a location where either heel or toe touches the ground initially and μ_s is the static frictional coefficient.

Otherwise, the horizontal reaction force is modeled as a dynamic friction force.

$$F_{gx}^i = -\mu_k F_{gy}^i \text{sgn}(\dot{x}^i) \quad (31)$$

where μ_k is the dynamic frictional coefficient.

Appendix C: Simulation parameter values

C.1. Normal walking

- Transmission neural delays

Closed-loop transmission delays are conservatively taken to be 60, 70, and 80 ms for long-loop response to and from the hip, knee, ankle, respectively based on 50 m/s neural conduction velocity, and five synaptic delays of less than 1 ms. Therefore, $\mathbf{T}_{spr} + \mathbf{T}_{sp} + \mathbf{T}_{pr} = [80 \ 70 \ 60]^T$. For simulation, $\mathbf{T}_{spr} = \mathbf{T}_{sp} + \mathbf{T}_{pr}$, $\mathbf{T}_{sp} = \mathbf{T}_{pr}$ are assumed. $EC(s)$ also lags neural signals.

- Foot interaction to the ground

$$K_{gy} = 30,000, \quad B_{gy} = 500, \quad K_{gx} = 10,000, \\ B_{gx} = 1,000; \quad \mu_k = 0.6, \quad \mu_s = 1.2.$$

- Spinal pattern generator

$$f_{PG} = 1.3 \quad \text{and} \quad m_{PG} = 1.2.$$

$$\mathbf{W}_{PG} = \begin{bmatrix} 0.3 & 0 & 0 & 0 & 0.8 & 0 & 0 & 0 & 0 \\ 0 & 0.29 & 0 & 0 & 0 & 0 & 0 & 0 & 0 \\ 0.4 & 0 & 0.64 & 0 & 0.9 & 0 & 0.35 & 0 & 0 \\ 0 & 0 & 0 & 0 & 0 & 0.4 & 0 & 0 & 0.3 \\ 0 & 0.1 & 0 & 0.8 & 0 & 0 & 0.4 & 0.1 & 0 \end{bmatrix}^T$$

(Table 2).

Table 2 Parameters for periodic pattern generation

| | $u_{PG,1}$ | $u_{PG,2}$ | $u_{PG,3}$ | $u_{PG,4}$ |
|----------|-----------------|----------------|-----------------|------------------|
| ϕ_i | 0.38 | 1.2 | 0.705 | 0.5275 |
| h_i | $\cos(0.16\pi)$ | $\cos(0.2\pi)$ | $\cos(0.23\pi)$ | $\cos(0.125\pi)$ |

• Spinal segmental inhibition

$$\theta_{th,a} = 0.35; \quad \theta_{th,k} = -0.35; \quad \theta_{th,h} = 0.55.$$

$$\mathbf{W}_{\text{reflex}} = \rho \begin{bmatrix} 0 & 0 & 0 & 0 & 1 & 0 & 0 & 0 & 0 \\ 0 & 0 & 1 & 0 & 0 & 0 & 0 & 0 & 0 \\ 1 & 0 & 0 & 0 & 0 & 0 & 0 & 0 & 0 \end{bmatrix}^T$$

where ρ is a sufficient large number ($\rho > m_{PG}$).

• Supraspinal system

Cerebro-cerebellar feedback control $i_a = 0.2, i_r = 100, f = 0.6, g_b = 0, g_k = 3,$

$$\mathbf{W}_C = [0 \quad 0 \quad 2 \quad -5 \quad 6 \quad -1 \quad 3 \quad -1 \quad -3]^T$$

Estimate of COM (\hat{x}_{com}): $p_1 = 0.97, p_2 = 0.53, p_3 = 0.14.$

• Vestibulospinal reflex feedback control

$$k_p = 3, \quad b_p = 0.9.$$

$$\mathbf{W}_{\text{ves}} = [0.132 \quad -0.092 \quad 0 \quad 0 \quad 0 \quad 0 \quad 0.049 \quad -0.054 \quad 0]^T$$

• Initial positions

$$\theta_a = 0.2, \theta_k = 0, \theta_h = -0.2 \quad \text{for right leg;}$$

$$\theta_a = 0, \theta_k = -0.1, \theta_h = 0.4 \quad \text{for left leg.}$$

• Initial velocities

$$\dot{\theta}_a = (f_{PG} + 1)/2, \dot{\theta}_k = -(f_{PG} + 1)/2,$$

$$\dot{\theta}_h = (f_{PG} + 1)/2 \quad \text{for right leg;}$$

$$\dot{\theta}_a = -(f_{PG} + 1)/2, \dot{\theta}_k = (f_{PG} + 1)/2,$$

$$\dot{\theta}_h = -(f_{PG} + 1)/2 \quad \text{for left leg.}$$

• Reference signals

$$u_{\text{ref}} = 0.25; \quad \theta_{\text{tr,ref}} = 0.$$

C.2. Forward bent walking

Other parameters are the same as in two except the followings:

• Initial positions

$$\theta_a = 0.2, \theta_k = 0, \theta_h = 0.7 \quad \text{for right leg;}$$

$$\theta_a = 0, \theta_k = -0.1, \theta_h = 1.3 \quad \text{for left leg.}$$

• Reference signals

$$\theta_{\text{tr,ref}} = 0.7.$$

• Neuronal network of spinal pattern generation

$$\mathbf{W}_{PG} = \begin{bmatrix} 0.4 & 0 & 0 & 0 & 0 & 0.1 & 0 & 0.4 & 0.2 \\ 0 & 0.3 & 0.5 & 0 & 0 & 0 & 0 & 0.3 & 0.2 \\ 0.5 & 0 & 0.64 & 0 & 1.0 & 0 & 0.35 & 0 & 0 \\ 0 & 0 & 0 & 0 & 0 & 0.1 & 0 & 0.2 & 0 \\ 0.4 & 0.1 & 0 & 0.8 & 0 & 0 & 0.4 & 0.1 & 0 \end{bmatrix}^T$$

References

1. Armstrong DM, Edgley SA (1988) Discharges of interpositus and Purkinje cells of the cat cerebellum during locomotion under different conditions. *J Physiol* 400:425–445
2. Brand RA, Pedersen DR, Friederich JA et al (1986) The sensitivity of muscle force predictions to changes in physiological cross-sectional area. *J Biomech* 8:589–596
3. Brooke JD, Cheng J, Collins DF, et al (1997) Sensori-sensory afferent conditioning with leg movement: gain control in spinal reflex and ascending paths. *Prog Neurobiol* 51:393–421
4. Cajigas González I (2003) Linear control model of the spinal processing of descending neural signals, Master’s thesis, Massachusetts Institute of Technology, Cambridge, MA
5. Calancie B, Needham-Shropshire B, Jacobs P et al (1994) Involuntary stepping after chronic spinal cord injury: evidence for a central rhythm generator for locomotion in man. *Brain* 117:1143–1159
6. Collins JJ, Stewart I (1994) A group-theoretic approach to rings of coupled biological oscillators. *Biol Cybern* 71:95–103
7. Crespi A, Badertscher A, Guignard A, Ijspeert AJ (2005) Amphibot I: an amphibious snake-like robot. *Robot Auto Sys* 50:163–175
8. d’Avella A, Satiel P, Bizzi E (2003) Combinations of muscle synergies in the construction of a natural motor behavior. *Nat Neurosci* 6(3):300–308
9. Dimitrijevic MR, Gerasimenko Y, Pinter MM (1998) Evidence for a spinal central pattern generator in humans. *Ann NY Acad Sci* 860:360–376
10. Dietz V (1992) Human neuronal control of automatic functional movements: interaction between central programs and afferent input. *Physiol Rev* 72(1):33–69
11. Dietz V, Harkema J (2004) Locomotor activity in spinal cord-injured persons. *J Appl Physiol* 96:1954–1960
12. Flash T (1987) The control of hand equilibrium trajectories in multi-joint arm movements. *Biol Cybern* 57:257–274
13. Fuglevand AJ, Winter DA (1993) Models of recruitment and rate coding organization in motor-unit pools. *J Neurophysiol* 70(6):2470–2488
14. Fujita K, Sato H (1998) Intrinsic viscoelasticity of ankle joint during standing. In: Proceedings of the 20th annual international conference of the IEEE engineering in medicine and biology society 20(5):2343–2345
15. Fukuoka Y, Kimura H, Cohen AH (2003) Adaptive dynamic walking of a quadruped robot on irregular terrain based on biological concepts. *Int J Robot Res* 22(3–4):187–202

16. Georgopoulos AP (1988) Neural integration of movement: role of motor cortex in reaching. *FASEB J* 2:2849–2857
17. Grasso R, Zago M, Lacquaniti F (2000) Interactions between posture and locomotion: motor patterns in humans walking with bent posture versus erect posture. *J Neurophysiol* 83:288–300
18. Huffman KJ, Krubitzer L (2001) Thalamo-cortical connections of area 3a and M1 in marmoset monkeys. *J Comp Neurol* 435(3):291–310
19. Inman VT, Ralston HJ, Todd F (1981) Human walking. In: Lieberman JC (ed) Williams & Wilkins, Baltimore, pp 41–55
20. Ito M (1997) Cerebellar microcomplexes. In: Schmähmann JD (ed) The cerebellum and cognition, vol 41. Academic, New York, pp 475–487
21. Ivanenko YP, Cappellini G, Dominici N et al (2005) Coordination of locomotion with voluntary movements in humans. *J Neurosci* 25(31):7238–7253
22. Ivanenko YP, Poppele RE, Lacquaniti F (2006) Spinal cord maps of spatiotemporal alpha-motoneuron activation in humans walking at different speeds. *J Neurophysiol* 95:602–618
23. Iwasaki T, Zhen M (2006) Sensory feedback mechanism underlying entrainment of central pattern generator to mechanical resonance. *Biol Cybern* 94(4):245–261
24. Jo S, Massaquoi SG (2004) A model of cerebellum stabilized and scheduled hybrid long-loop control of upright balance. *Biol Cybern* 91:188–202
25. Jo S, Massaquoi SG (2007) A model of cerebrocerebello-spino-muscular interaction in the sagittal control of human walking. *Biol Cybern* 96
26. Karameh FN, Massaquoi SG (2005) A model of nonlinear motor cortical integration and its relation to movement speed profile control. In: Proceedings 2005 IEEE Engineering in Medicine and Biology, 27th Annual conference, Shanghai, China, Sept 1–4
27. Katayama M, Kawato M (1993) Virtual trajectory and stiffness ellipse during multijoint arm movement predicted by neural inverse models. *Biol Cybern* 69:353–362
28. Lacquaniti F, Soechting JF (1986) Simulation studies on the control of posture and movement in a multi-jointed limb. *Biol Cybern* 54:367–378
29. Massaquoi SG (1999) Modelling the function of the cerebellum in scheduled linear servo control of simple horizontal planar arm movements. Electrical Engineering & Computer Science, Massachusetts Institute of Technology, Cambridge, MA
30. Massaquoi SG, Topka H (2002) Models of cerebellar function. In: Pandolfo M, Manto M (eds) The cerebellum and its disorders. Cambridge University Press, Cambridge, pp 69–94
31. Matarić MJ (2002) Sensory-motor primitives as a basis for imitation: linking perception to action and biology to robotics. In: Dautenhahn K, Nehaniv C (eds) Imitation in animals and artifacts. MIT, Cambridge, pp 392–422
32. Mori S, Nakajima K, Mori F, Matsuyama K (2004) Integration of multiple motor segments for the elaboration of locomotion: role of the fastigial nucleus of the cerebellum. *Prog Brain Res* 143:341–351
33. Nathan PW (1994) Effects on movement of surgical incisions into the human spinal cord. *Brain* 117(Pt2):337–346
34. Ogihara N, Yamazaki N (2001) Generation of human bipedal locomotion by a bio-mimetic neuro-musculo-skeletal model. *Biol Cybern* 84:1–11
35. Rossignol S, Dubbue R, Gossard J-P (2006) Dynamic sensori-motor interaction in locomotion. *Physiol Rev* 86:89–154
36. Rudomin P, Schmidt RF (1999) Presynaptic inhibition in the vertebrate spinal cord revisited. *Exp Brain Res* 129(1):1–37
37. Saltiel P, Wyler-Duda K, d’Avella A, et al (2001) Muscle synergies encoded within the spinal cord: evidence from focal intraspinal NMDA iontophoresis in the frog. *J Neurophysiol* 85:605–619
38. Shik ML, Orlovsky GN (1976) Neurophysiology of locomotor automatism. *Physiol Rev* 56(3):465–501
39. Taga G (1995) A model of the neuro-musculo-skeletal system for human locomotion I. Emergence of basic gait. *Biol Cybern* 73:97–111
40. Taga G (1998) A model of the neuro-musculo-skeletal system for anticipatory adjustment of human locomotion during obstacle avoidance. *Biol Cybern* 78:9–17
41. Thach WT, Goodlin HP, Keating JG (1992) The cerebellum and the adaptive coordination of movement. *Annu Rev Neurosci* 15:403–442
42. Tresch MC, Salteit P, Bizzi E (1999) The construction of movement by the spinal cord. *Nat Neurosci* 2:162–167
43. Winter DA (1990) Biomechanics and motor control of human movement, 2nd edn. Wiley, New York